Received: 11 December 2023 | Revised: 25 January 2024 | Accepted: 14 February 2024

DOI: 10.1111/clr.14252

ORIGINAL ARTICLE

CLINICAL ORAL IMPLANTS RESEARCH WILEY

Accuracy of edentulous full-arch implant impression: An in vitro comparison between conventional impression, intraoral scan with and without splinting, and photogrammetry

Jing Cheng[1] | Haidong Zhang[2] | Hailin Liu[3] | Junying Li[4] | Hom-Lay Wang[5] | Xian Tao[6]

[1]Department of General Dentistry, Stomatological Hospital of Xiamen Medical College, Xiamen Key Laboratory of Stomatological Disease Diagnosis and Treatment, Xiamen, China

[2]Department of Periodontology, Peking University School and Hospital of Stomatology & National Center of Stomatology & National Clinical Research Center for Oral Diseases & National Engineering Laboratory for Digital and Material Technology of Stomatology, Beijing, China

[3]Jingpin Medical Technology (Beijing) Company Limited, Beijing, China

[4]Department of Biologic and Materials Sciences & Prosthodontics, University of Michigan School of Dentistry, Ann Arbor, Michigan, USA

[5]Department of Periodontics and Oral Medicine, University of Michigan School of Dentistry, Ann Arbor, Michigan, USA

[6]Department of Prosthodontics, Stomatological Hospital of Xiamen Medical College, Xiamen Key Laboratory of Stomatological Disease Diagnosis and Treatment, Xiamen, China

Correspondence

Hom-Lay Wang, Department of Periodontics and Oral Medicine, The University of Michigan School of Dentistry, 1011 North University Avenue, Ann Arbor, MI 48109-1078, USA.
Email: homlay@umich.edu

Xian Tao, Department of Prosthodontics, Stomatological Hospital of Xiamen Medical College, No.1309, Lvling Road, Huli District, Xiamen, Fujian 361008, China.
Email: taoxian19870817@126.com

Funding information

Natural Science Foundation of Xiamen, China, Grant/Award Number: 3502Z202373149 and 3502Z202372106; Foundation of Stomatological Hospital of Xiamen Medical College, Grant/Award Number: 2023XKQN0009

Abstract

Objectives: The purpose of this in vitro study was to compare the trueness and precision of complete arch implant impressions using conventional impression, intraoral scanning with and without splinting, and stereophotogrammetry.

Materials and Methods: An edentulous model with six implants was used in this study. Four implant impression techniques were compared: the conventional impression (CI), intraoral scanning (IOS) without splinting, intraoral scanning with splinting (MIOS), and stereophotogrammetry (SPG). An industrial blue light scanner was used to generate the baseline scan from the model. The CI was captured with a laboratory scanner. The reference best-fit method was then applied in the computer-aided design (CAD) software to compute the three-dimensional, angular, and linear discrepancies among the four impression techniques. The root mean square (RMS) 3D discrepancies in trueness and precision between the four impression groups were analyzed with a Kruskal–Wallis test. Trueness and precision between single analogs were assessed using generalized estimating equations.

Results: Significant differences in the overall trueness ($p = .017$) and precision ($p < .001$) were observed across four impression groups. The SPG group exhibited significantly smaller RMS 3D deviations than the CI, IOS, and MIOS groups ($p < .05$), with no significant difference detected among the latter three groups ($p > .05$).

Jing Cheng and Haidong Zhang contributed equally to this article.

Conclusions: Stereophotogrammetry showed superior trueness and precision, meeting misfit thresholds for implant-supported complete arch prostheses. Intraoral scanning, while accurate like conventional impressions, exhibited cross-arch angular and linear deviations. Adding a splint to the scan body did not improve intraoral scanning accuracy.

KEYWORDS
accuracy, digital impression, intraoral scanning, stereophotogrammetry

1 | INTRODUCTION

Implant-supported complete arch prostheses, a common edentulous patient treatment, have a survival rate of 83.8% to 96% (Jemt, 2018; Lambert et al., 2009; Papaspyridakos et al., 2014). Misfitting can lead to mechanical issues like screw problems and fractures (al-Turki et al., 2002; Jemt, 2017; Katsoulis et al., 2017; Pan et al., 2021; Toia et al., 2019), emphasizing the need for a passive fit (Daudt Polido et al., 2018; Pan et al., 2021; Slauch et al., 2019). Achieving this passive fit relies on accurately transferring implant positions to the model during impressions (Filho et al., 2009).

Conventional implant impression procedures often use an open-tray technique with impression copings splinting. While reasonably accurate, this method is time-consuming and labor-intensive (Dounis et al., 1991). With the advent of computer-aided design and computer-aided manufacturing (CAD-CAM) technology in dentistry, digital impressions are increasingly replacing conventional techniques for fixed implant restorations in edentulous jaws. Intraoral scan (IOS) allows for 3D models directly from a patient's mouth, eliminating the need for traditional impressions. This approach streamlines the digital workflow, reducing potential inaccuracies like material expansion, shrinkage, or distortion (Patzelt et al., 2014).

Intraoral scans are gaining popularity due to improved patient comfort and efficiency in clinical practice (de Oliveira et al., 2020; Gallardo et al., 2018; Yuzbasioglu et al., 2014). However, the accuracy of intraoral scanners can be influenced by factors such as ambient light, scanner brand, scan body type, range, and pattern (Arcuri et al., 2022; Fluegge et al., 2017; Imburgia et al., 2017; Mizumoto et al., 2020; Müller et al., 2016; Ochoa-López et al., 2022; Pan et al., 2020; Schimmel et al., 2021). Some propose enhancing accuracy by adding soft tissue landmarks or geometric devices to scan bodies (Arikan et al., 2023; Iturrate et al., 2019; Masu et al., 2021), while others argue that even with these additions, digital impressions for complete arches may be less accurate than conventional impressions (CIs) (Pan et al., 2022). To further enhance accuracy for complete arch digital impressions involving multiple implants, ongoing technological advancements are needed (Gaikwad et al., 2022; Zhang et al., 2021).

Since the 1990s, photogrammetric techniques have seen increasing use in edentulous jaw implant impressions (Jemt et al., 1999). The emergence of commercial stereophotogrammetric systems has transformed this method into a new approach for creating impressions. Although numerous clinical reports confirm the ability of stereophotogrammetry (SPG) to accurately transfer intraoral implant positions to a virtual model, there has been inconsistency in study findings regarding SPG's accuracy (Bratos et al., 2018; Peñarrocha-Oltra et al., 2017; Revilla-León et al., 2021; Sallorenzo & Gómez-Polo, 2022; Sánchez-Monescillo et al., 2016; Tohme et al., 2023; Zhang et al., 2023). Currently, a lack of comparative studies on various digital edentulous implant impression techniques raises doubts about their potential to enhance impression accuracy. Therefore, additional in vivo and in vitro studies are needed to address these concerns comprehensively.

The assessment of implant impression accuracy involves two key aspects: trueness and precision (ISO 5725-1, 1994). Trueness measures the variance between baseline data and test data, while precision assesses the method's repeatability. In this study, we examined the three-dimensional, linear, and angular discrepancies of four impression techniques: CI, standard intraoral scanning (IOS), intraoral scanning with splinting (MIOS), and SPG in a maxillary edentulous jaw with six implants. The objective was to compare the accuracy of these four methods, with the null hypothesis suggesting no statistical differences among them.

2 | MATERIALS AND METHODS

This study has been followed strengthening the reporting of observational studies in epidemiology (STROBE) Statement (Appendix S1). Ethics approval was not required for this in vitro study. The maxillary edentulous standard model underwent remodeling using professional CAM software (hyperMill 2022.1, Openmind). This process generated a sectionalized model at 2 and 3 mm increments, encompassing the upper soft tissue base and the lower metal arch base. Subsequently, these sections were milled from an aerospace-grade aluminum block using a five-axis milling machine (HSC300-5, QIRUN). To facilitate implant placement, 3 mm diameter, 20 mm depth cylindrical holes were strategically engineered at the sites corresponding to #3, #5, #7, #10, #12 and #14 of the arch base (Figure 1a). Following sequential cavity preparation at the designated implant sites, six implants (bSKY4012, SKY) were inserted (Figure 1b,c). Each implant was fitted with a multiunit abutment (SKYUC003, SKY) and tightened to 25 Ncm using a calibrated cordless restorative screwdriver (IA-400, SKY). The soft tissue component of the removable

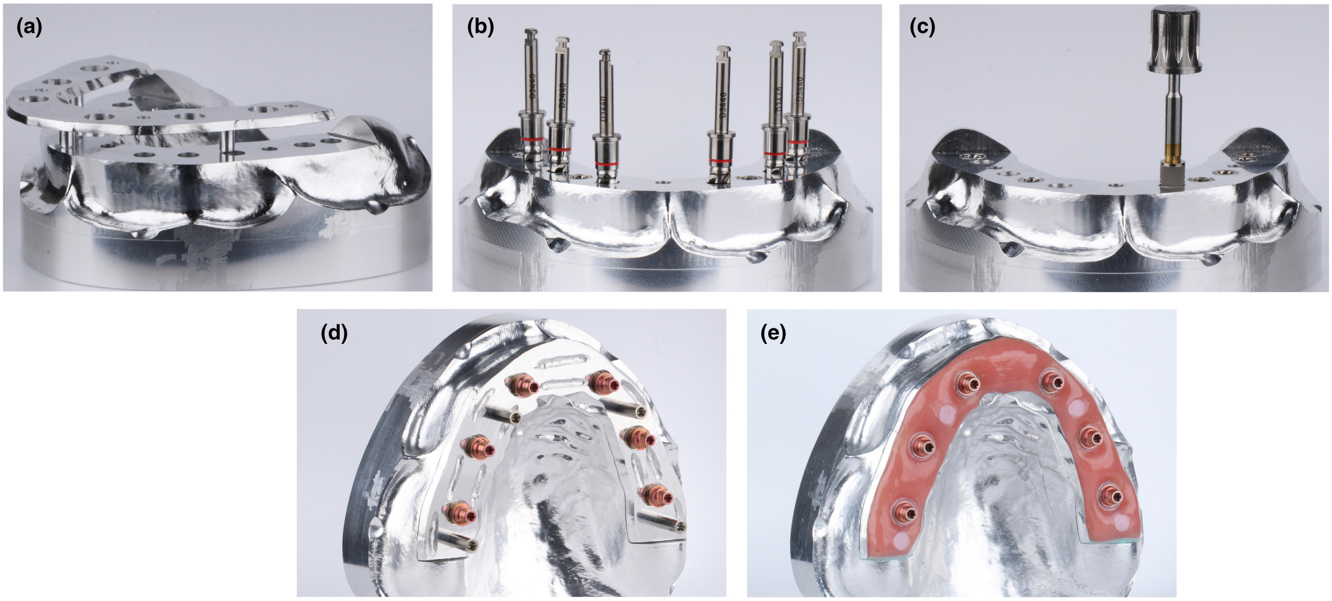

FIGURE 1 The process of making a master model. (a) The master model, made from an aerospace-grade aluminum alloy, was constructed with CAD/CAM techniques. (b) Sequential cavity preparation occurred at the sites of both lateral incisors, first premolars and first molars. (c) lacement of six implants following cavity preparation. (d) Attachment of right-angled multiunit abutments to the implants, tightened at 25 Ncm. (e) Mounting of fluid resin generated artificial soft tissue.

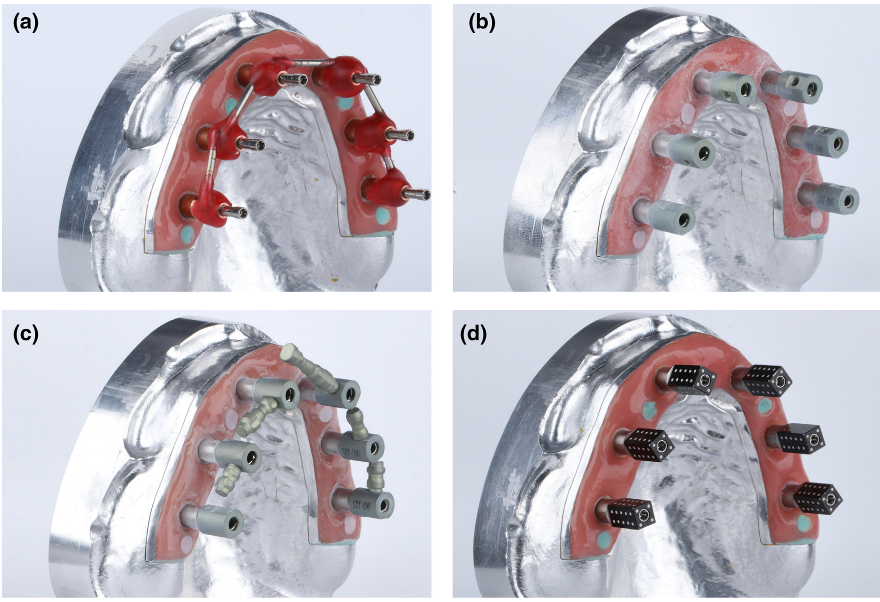

FIGURE 2 The process of producing four types of impressions. (a) Conventional impression. (b) Standard intraoral scanning. (c) Intraoral scanning with splinting. (d) Stereophotogrammetry.

edentulous arch was created by combining fluid resin (crea.Lign, BREDENT) with the metal soft tissue base (Figure 1d,e). Finally, the aerospace aluminum alloy master model was scanned with an industrial blue light scanner (ATOS Capsule 12 m, ATOS) following manufacturer's guidelines, yielding the 3D data of the master model.

For the conventional open-tray impressions technique, the impression copings (SKYUCAOL, SKY) were placed on the multi-unit abutment and securely tightened at 10 Ncm using a cordless screwdriver. Subsequently, 15 mm metal connecting rods were placed between adjacent impression copings and held in place with self-consolidating acrylic resin (Unifast Trad, GC) (Figure 2a).

Subsequently, the model underwent scanning in a laboratory scanner (3shape D2000, 3shape) to produce three-dimensional data. This baseline model data were imported into the dental CAD software to facilitate the design of the custom tray, followed by 3D printing of these trays with acrylic resin in an 3D printer (A20, HEYGEARS). Impressions were created using a silicone rubber impression material (Silagum-Putty, DMG) using open-tray technique. Following this, a plaster model was poured using Type IV gypsum according to the manufacturer's guidelines. The procedures were repeated until 10 specimens were obtained. All stone castes were subsequently scanned using a laboratory scanner, yielding STL files.

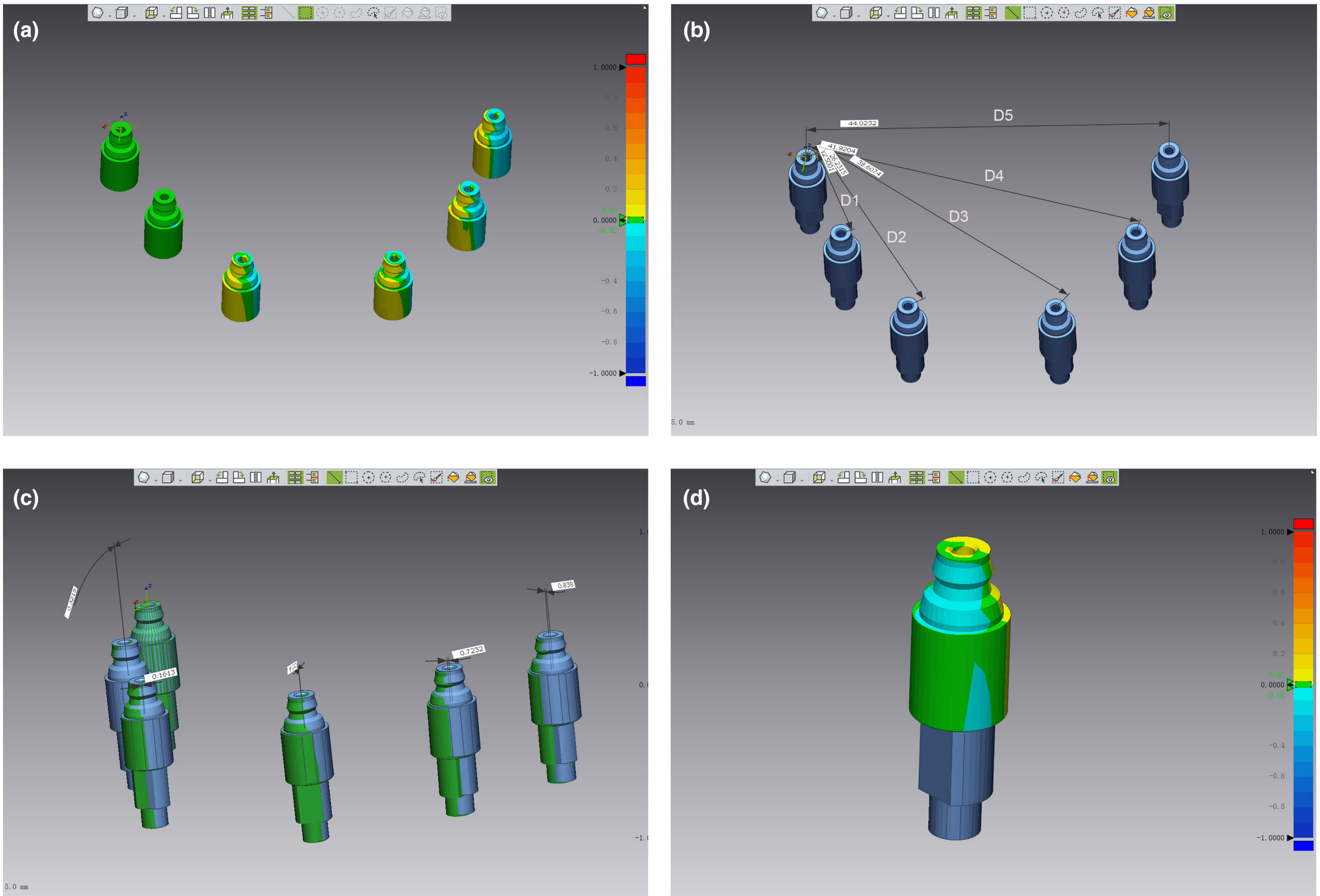

FIGURE 3 Trueness and precision measurements of RMS 3D deviation, linear deviation, and angular deviation for four impression techniques. (a) The calculation of 3D discrepancies for all analogs is represented with color plots to enhance visual understanding. (b) The distances between the analogs were measured to determine the absolute linear variation. (c) The angular deviation of the axes of two same-site analogs was computed. (d) The 3D variation of individual analogs was assessed.

TABLE 1 Summary of the RMS 3D deviation for trueness and precision of all analogs across the four impression techniques.

RMS 3D deviation (μm)	CI	IOS	MIOS	SPG	*p*
Trueness	87.3 (75.8, 120.9)[a]	79.6 (72.3, 102.4)[ab]	89.5 (61.5, 99.5)[ab]	69.2 (56.0, 75.0)[c]	.017
Precision	77.1 (58.8, 102.6)[a]	59.2 (46.9, 94.6)[ab]	73.4 (46.8, 126.1)[ab]	41.1 (22.0, 45.9)[c]	<.001

Note: The numbers in the table represent median (lower quartiles, upper quartiles). Different letters indicate significant difference between impression techniques from the Kruskal–Wallis test ($p<.05$).

Abbreviations: CI, conventional impression; IOS, intraoral scanning; MIOS, intraoral scanning with splinting; SPG, stereophotogrammetry.

For the standard IOS group, titanium implant scan bodies (Universal Scanbody, Segma) were placed on the multiunit abutment and were tightened to 10 Ncm (Figure 2b). The intraoral scanner (3shape TRIOS 3, 3shape) was calibrated according to the manufacturer's instructions. The scanning procedure was conducted by the same operator with an intraoral scanner following the manufacturer's prescribed scanning protocol. This scanning procedure involved a progression from the occlusal surface at #14 to #3, followed by the buccal surface and palatal surface. This process was repeated 10 times to yield a collection of 10 sets of intraoral scanning data in STL format.

The intraoral scanning with splinting (MIOS) group followed essentially the same procedure as the standard IOS group, with the following exceptions: (1) implant scan bodies with splinting (Multi Unit Scanbody, Segma) were placed to the multiunit abutment of the baseline cast and tightened to 10 Ncm. (2) Recalibration of the intraoral scanner to match the splinting in line with the manufacturer's directives (Figure 2c).

In the SPG group, the scan bodies (ICamBody, Imetric4D Imaging Sàrl) were affixed and hand-tightened to the multiunit abutment of the baseline cast, in accordance with the manufacturer's guidelines (Figure 2d). Utilizing the stereoradiographic system (ICam4D, Imetric4D Imaging Sàrl), the scan bodies were methodically scanned across the baseline cast from left to right, securing data on the implant's position and orientation across 10

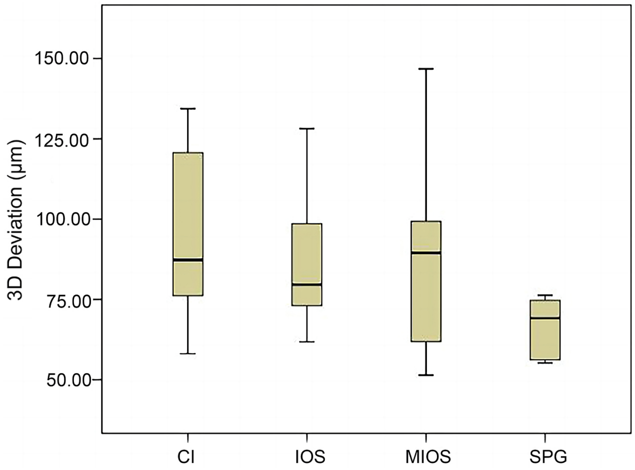

FIGURE 4 Comparing the 3D deviation in the trueness of all analogs across the four impression techniques.

scans. This positional data were then input into the dental CAD software, which facilitates the generation of the 3D data for the implants in STL format.

The four sets of modeling data obtained were imported into the dental CAD software, where the scan bodies were transformed into implant analogs and saved as STL files. These files were imported into a 3D software (Geomagic Wrap, 3D Systems) for measurement, where the apical center of the left first molar's analog was established as the coordinate system origin. The analogs of #14 from the four experimental groups were then superimposed onto the same analog of the master model using the "best-fit algorithm." This process ensures that the scanned data of the implant analogs of #14 all occupy the same position and are saved as STL files. The data were subsequently segmented into individual implant analogs, each saved as an STL file.

The comprehensive STL files, comprising all implant analogs, were imported into the measurement software (Geomagic control X,3D Systems). The upper cylinders of all analogs were selected for a 3D comparison. The root mean square (RMS) error was used to evaluate the overall 3D discrepancy between the baseline cast data and each of the datasets from the four impression techniques (Figure 3a). The center point of the implant analog was intersection between the axis of the analog and the apical plane. For each impression technique dataset, the center point of the implant analog of #14 was linked to the center points of the implant analogs of #12, #10, #7, #5 and #3, labeled as D1, D2, D3, D4, and D5, respectively (Figure 3b). This was to assess the linear differences between the baseline cast data and experimental impression data. Following this, the angles of the central axes of any two implant analogs at the same site were measured to assess the angular discrepancy between them (Figure 3c). The STL files of two same-site implant analogs were imported into the measurement software, and the apical cylinder of the analogs was selected for a 3D comparison. The RMS error was used to evaluate the 3D deviation for the two same-site implant analogs (Figure 3d). Trueness was evaluated by comparing the master model data with the experimental

TABLE 2 Summary of the RMS 3D deviation and angular deviation for trueness of the individual analog sites across the four impression techniques.

Trueness	Group	#12	#10	#7	#5	#3
RMS 3D deviation (μm)	CI	51.10 (39.18, 73.30)^{aB}	89.50 (78.80, 95.43)^{AB}	92.65 (80.95, 155.05)^{aA}	88.40 (61.95, 141.45)^{AB}	116.30 (94.68, 139.48)^{aA}
	IOS	50.40 (45.18, 57.95)^{aB}	90.95 (75.48, 118.40)^{A}	112.75 (100.33, 141.98)^{aA}	69.75 (55.28, 83.60)^{AB}	85.10 (55.98, 108.35)^{abAB}
	MIOS	28.30 (24.50, 38.43)^{bB}	86.45 (76.18, 123.00)^{A}	114.40 (69.95, 131.10)^{abA}	112.10 (58.20, 130.75)^{A}	103.60 (77.18, 114.73)^{abA}
	SPG	37.15 (34.23, 43.30)^{abB}	97.30 (80.80, 111.53)^{A}	71.95 (61.00, 79.93)^{bAC}	61.70 (49.38, 76.50)B^{C}	75.40 (45.68, 91.40)^{bAB}
	p	<.001	.893	.022	.193	.018
Angular deviation (degrees)	CI	0.41 (0.31, 0.58)^{ab}	0.53 (0.39, 0.76)^{bc}	0.56 (0.49, 0.66)a	0.73 (0.55, 0.82)^{ab}	0.58 (0.27, 0.66)^{ab}
	IOS	0.42 (0.29, 0.54)^{aB}	0.96 (0.62, 1.13)^{aA}	0.65 (0.56, 0.78)^{aAB}	0.75 (0.60, 0.80)^{aAB}	0.68 (0.55, 0.76)^{aAB}
	MIOS	0.64 (0.55, 0.72)^{bAB}	0.83 (0.73, 0.92)^{acB}	0.65 (0.48, 0.69)^{aA}	0.61 (0.50, 0.66)^{abA}	0.65 (0.54, 0.71)^{aAB}
	SPG	0.39 (0.36, 0.44)^{aABC}	0.54 (0.52, 0.64)^{bB}	0.27 (0.23, 0.30)^{bA}	0.42 (0.37, 0.52)^{bBC}	0.34 (0.30, 0.36)^{bAC}
	p	.006	.002	<.001	.021	.002

Note: The numbers in the table represent median (lower quartiles, upper quartiles). The lowercase letters represent comparisons within the same site but two different groups, while the uppercase letters illustrate comparisons within the same group but across different sites. Different letters indicate a statistically significant difference ($p < .05$).

Abbreviations: CI, conventional impression; IOS, intraoral scanning; MIOS, intraoral scanning with splinting; SPG, stereophotogrammetry.

group data, whereas precision was assessed through pairwise comparisons within the experimental groups.

Statistical evaluation was performed using the SPSS analysis software program (IBM SPSS Statistic, v26.0, IBM Corp). The Shapiro–Wilk test confirmed the absence of normal data distribution. Consequently, the Kruskal–Wallis test was used to assess the trueness and precision of the overall RMS 3D discrepancies between the four impression groups. The general comparison of trueness and precision among individual analogs was evaluated using the generalized estimating equations (GEE) method. The Kruskal–Wallis test allowed for comparisons between different groups using the same analog, while the Friedman test facilitated comparisons within the same groups across various analogs. The significance level was set at $\alpha = 0.05$.

3 | RESULTS

Regarding trueness, a significant difference was observed of in overall comparison of the RMS 3D discrepancies and angular deviation among groups, sites, and interaction ($p < .05$). Stereophotogrammetry consistently exhibited smaller RMS 3D differences for all analogs compared to the CI, intraoral scanning (IOS), and intraoral scanning with splinting (MIOS) (Table 1 and Figure 4). Analyzing the RMS 3D discrepancies for each impression technique at the individual analog level revealed that SPG data exhibited reduced bias for #7 and #3, while the MIOS group demonstrated the same for #12 ($p < .05$) (Table 2 and Figure 5). Among all experimental groups, the minimum 3D bias was observed at the analog of #12 ($p < .05$; Table 2 and Figure 5). The angular bias was the least for SPG at the analogs of #7, #5, and #3, and for the MIOS group at the analog of #12 ($p < .001$; Table 2 and Figure 6). MIOS displayed a larger angular deviation at the analog of #12 compared to the other three groups ($p < .001$; Table 2 and Figure 6). In terms of linear error, the deviation at D4 (between #14 and #5) was larger for SPG than the other groups and smallest for the MIOS group ($p = .002$; Table 4 and Figure 7). The CI group showed smaller linear errors at D4 compared to D1 (between #14 and #12), while the IOS and MIOS groups showed larger linear errors at D3 (between #14 and #7) ($p < .05$; Table 4 and Figure 7). For the SPG group, larger linear errors were found at D3 and D4 ($p < .05$; Table 4 and Figure 7).

Regarding precision, a statistically significant difference was observed in overall comparison of the RMS 3D deviations and angular deviations among groups, sites, and interaction ($p < .001$). The SPG group exhibited significantly smaller RMS 3D deviations than the CI, IOS, and MIOS groups, with no significant difference detected among the latter three groups (refer to Table 1 and Figure 8). Upon analyzing the RMS 3D deviation for each impression technique at the individual analog level, the SPG group displayed the smallest 3D deviation at all implant analogs ($p < .001$; Table 3 and Figure 9). Across all impression techniques, the least 3D deviation was observed at the analog of #12 ($p < .001$; Table 3 and Figure 9). The SPG group also showed smaller angular deviations at all analogs compared to the other groups ($p < .001$; Table 3 and Figure 10). With regard to linear deviations, the CI and IOS groups demonstrated smaller deviations at D5 (between #14 and #3), while the MIOS and SPG groups exhibited smaller deviations at D1 (between #14 and the #12; $p < .001$; Table 4 and Figure 11).

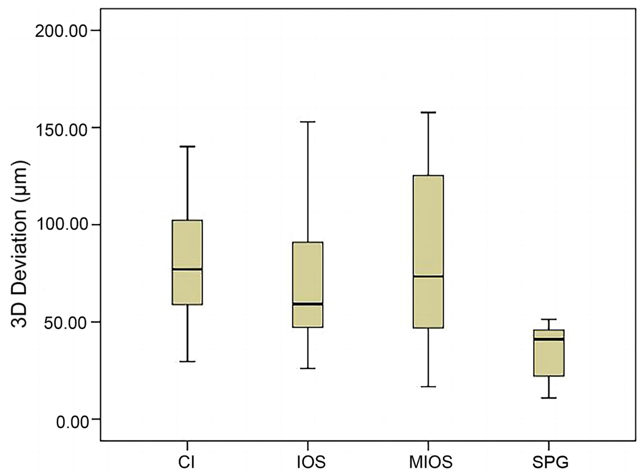

FIGURE 5 Comparing the 3D deviation in the precision of all analogs across the four impression techniques.

FIGURE 6 Comparing the 3D deviation in trueness of the individual analog sites across the four impression techniques.

TABLE 3 Summary of the RMS 3D deviation and angular deviation for the precision of the individual implant sites across the four impression techniques.

Precision	Group	#12	#10	#7	#5	#3
RMS 3D deviation (μm)	CI	41.20 (22.75, 62.00)^{aC}	71.50 (47.50, 93.10)^{aA}	111.20 (73.20, 138.55)^{aB}	91.60 (62.65, 126.20)^{aAB}	74.10 (52.20, 110.75)^{aA}
	IOS	36.90 (24.45, 55.60)^{aB}	57.00 (38.05, 94.50)^{aA}	69.40 (49.25, 83.20)^{bA}	67.60 (50.55, 92.35)^{aA}	71.90 (45.20, 117.30)^{aA}
	MIOS	36.50 (28.45, 44.95)^{aC}	57.70 (42.15, 89.60)^{aB}	89.30 (58.85, 182.15)^{aA}	95.90 (51.30, 175.85)^{aA}	89.10 (46.10, 144.25)^{aA}
	SPG	17.10 (12.25, 21.65)^{bC}	34.20 (22.05, 48.10)^{bB}	53.50 (23.70, 62.50)^{cAB}	36.80 (25.25, 52.50)^{bAB}	49.50 (34.25, 57.70)^{bA}
	p	<.001	<.001	<.001	<.001	<.001
Angular deviation (degrees)	CI	0.30 (0.20, 0.51)^{aB}	0.45 (0.32, 0.56)^{aAB}	0.47 (0.27, 0.83)^{aA}	0.44 (0.28, 0.56)^{aAB}	0.36 (0.24, 0.57)^{aAB}
	IOS	0.23 (0.15, 0.34)^{aA}	0.41 (0.27, 0.61)^{aB}	0.28 (0.19, 0.44)^{aAB}	0.26 (0.19, 0.36)^{abA}	0.33 (0.19, 0.45)^{abA}
	MIOS	0.20 (0.11, 0.30)^{aA}	0.25 (0.14, 0.34)^{bAC}	0.37 (0.21, 0.60)^{aB}	0.31 (0.17, 0.42)^{bBC}	0.23 (0.12, 0.34)^{bAC}
	SPG	0.13 (0.08, 0.20)^{bA}	0.18 (0.09, 0.26)^{bAB}	0.13 (0.09, 0.19)^{bA}	0.22 (0.14, 0.30)^{bB}	0.15 (0.10, 0.19)^{cA}
	p	<.001	<.001	<.001	<.001	<.001

Note: The numbers in the table represent median (lower quartiles, upper quartiles). The lowercase letters represent comparisons within the same site but across two groups, while the uppercase letters illustrate comparisons within the same group but across two different sites. Different letters indicate a statistically significant difference ($p < .05$). CI, conventional impression; IOS, intraoral scanning; MIOS, intraoral scanning with splinting; SPG, stereophotogrammetry.

TABLE 4 Summary of the linear deviation of trueness and precision between the left first molar and the individual implant sites across the four impression techniques.

Linear deviation (μm)	Group	D1	D2	D3	D4	D5
Trueness	CI	44.15 (38.95, 63.48)^{aB}	25.70 (10.33, 40.15)^{AB}	45.65 (33.85, 55.20)^{AB}	14.05 (10.97, 55.75)^{aA}	38.05 (23.32, 98.07)^{AB}
	IOS	32.30 (25.80, 48.63)^{abA}	30.00 (18.25, 49.32)^{A}	80.20 (62.83, 110.98)^{B}	32.15 (16.45, 64.45)^{aA}	16.10 (12.82, 53.70)^{A}
	MIOS	8.00 (4.12, 18.40)^{bB}	17.15 (14.28, 36.73)^{B}	76.55 (61.10, 92.05)^{A}	28.90 (10.75, 55.27)^{aAB}	43.55 (20.73, 64.42)^{AB}
	SPG	55.40 (51.60, 71.78)^{aABC}	54.45 (11.83, 73.65)^{AC}	79.80 (20.15, 109.95)^{BC}	93.05 (85.25, 111.05)^{bB}	28.35 (11.10, 55.70)^{A}
	p	<.001	.412	.079	.002	.210
Precision	CI	17.10 (10.05, 28.15)^{abB}	31.00 (16.70, 55.45)^{aB}	18.90 (7.55, 31.35)^{aB}	27.70 (13.70, 108.30)^{aAB}	59.60 (20.15, 132.25)^{acA}
	IOS	21.00 (8.25, 35.20)aB	27.20 (13.40, 46.35)aAB	37.50 (17.70, 66.90)^{bA}	31.30 (16.70, 49.10)^{abAB}	37.40 (22.60, 69.15)^{bcA}
	MIOS	13.50 (6.95, 23.20)^{abC}	17.70 (3.40, 24.90)^{bC}	28.20 (10.95, 48.05)^{abB}	37.30 (20.85, 71.30)^{aAB}	65.60 (32.45, 109.35)^{aA}
	SPG	11.80 (4.50, 18.50)^{bC}	41.30 (14.80, 66.50)^{aA}	50.10 (15.85, 84.60)^{bB}	15.00 (6.55, 45.95)^{bA}	37.40 (15.60, 59.05)^{bA}
	p	<.001	<.001	<.001	.002	<.001

Note: The numbers in the table represent median (lower quartiles, upper quartiles). The lowercase letters represent comparisons within the same site but across two different groups, while the uppercase letters illustrate comparisons within the same group but across two different sites. Different letters indicate a statistically significant difference ($p < .05$). D1, between #14 to #12; D2, between #14 to#10; D3, between #14 to #7; D4, between #14 to #5; D5, between #14 to #3.

Abbreviations: CI, conventional impression; IOS, intraoral scanning; MIOS, intraoral scanning with splinting; SPG, stereophotogrammetry.

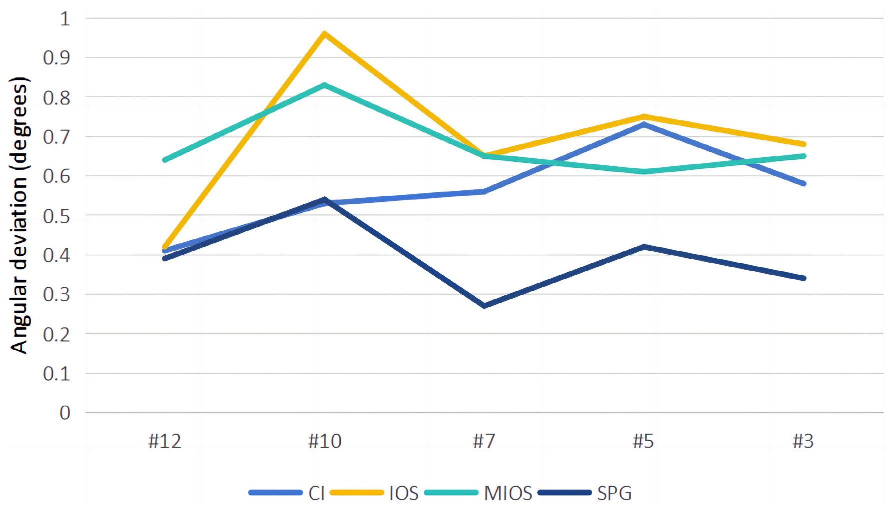

FIGURE 7 Comparing the angular deviation in trueness of the individual analog sites across the four impression techniques.

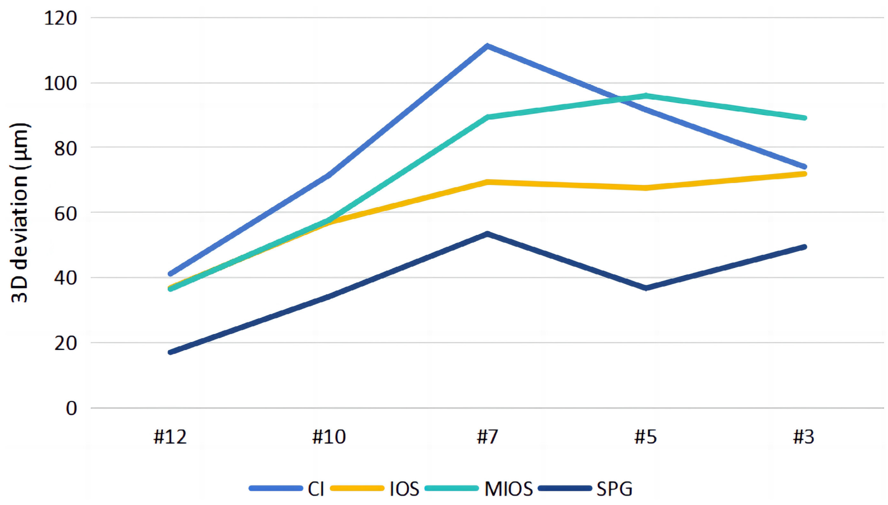

FIGURE 8 Comparing the 3D deviation in precision of the individual analog sites across the four impression techniques.

4 | DISCUSSION

This study evaluated the accuracy of four impression techniques: conventional, standard intraoral scanning, intraoral scanning with splinting, and stereophotogrammetry for generating the implant-supported fixed complete arch prostheses. The null hypothesis, suggesting no difference among the four impression techniques, was rejected. Significant disparities were noted across the techniques in terms of the trueness and precision of all analogs, as manifested in three-dimensional and linear deviations. Additionally, significant variations were detected in the trueness and precision of individual analogs, particularly in three-dimensional and angular deviations.

For the present investigation, an aerospace-grade aluminum alloy was employed to construct the maxillary edentulous jaw baseline cast, thus addressing the issues of wear, fracture, and deformation often encountered in repetitive impression manufacturing. Historically, research has predominantly utilized stone or resin cast, both of which are susceptible to fracture, wear, and deformation throughout the experimental process (Ellakany et al., 2022; Jin et al., 2019). Notably, stone cast only maintain stability for about 10 days (Hamm et al., 2020). However, aerospace-grade aluminum alloy offers superior attributes such as enhanced strength, fracture resistance, dimensional stability, and stress corrosion resistance, making it an optimal material for master models (Zhou et al., 2021). While most preceding studies have embedded substitutes into the master model to simulate a patient's intraoral implant condition (Kosago et al., 2022; Ma et al., 2021; Ortorp et al., 2005; Revilla-León et al., 2023; Tohme et al., 2023), the present investigation deviated by directly inserting dental implants into the baseline cast, thus more closely mirroring actual clinical scenarios. Furthermore, a metal base was designed to ensure the stability of the simulated gingiva during repeated removal, enhancing the reliability of the results.

Presently, the assessment of implant accuracy primarily employs methods such as the best-fit algorithm, the absolute linear deviation, and the angular deviation. The standard best-fit algorithm utilizes the Iterative Closest Point (ICP) algorithm for scanning. This algorithm aligns by minimizing the mesh distance error among each corresponding data point. Inherent in the termination criteria of this iterative algorithm is the ability to evenly distribute errors between positive and negative deviations, reducing the mesh distance errors.

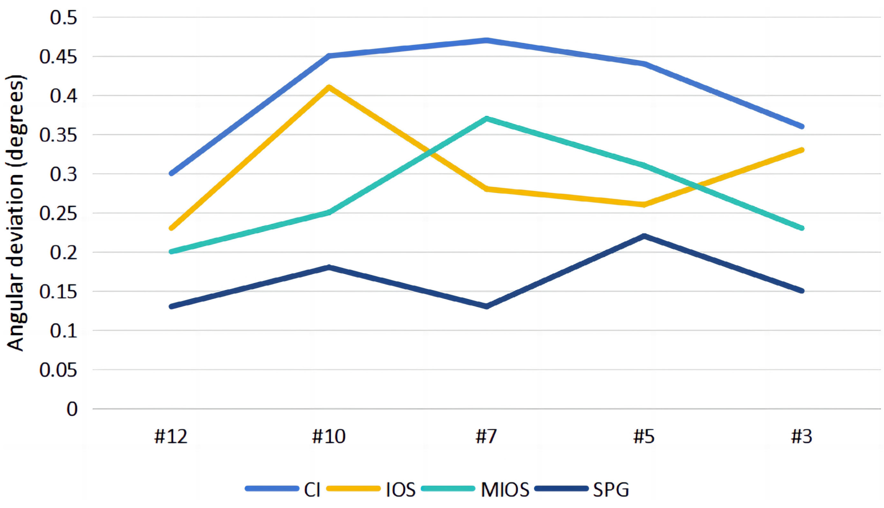

FIGURE 9 Comparing the angular deviation in precision of the individual analog sites across the four impression techniques.

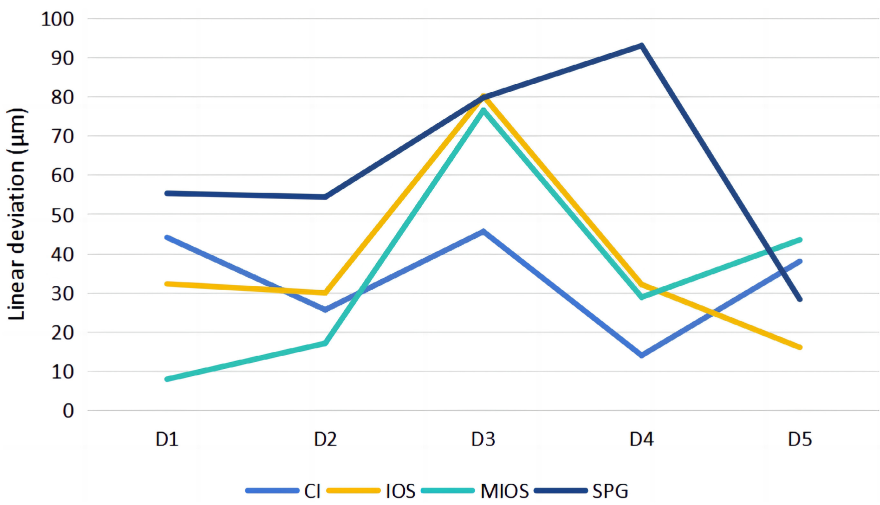

FIGURE 10 Comparing the linear deviation in trueness of the individual analog sites across the four impression techniques.

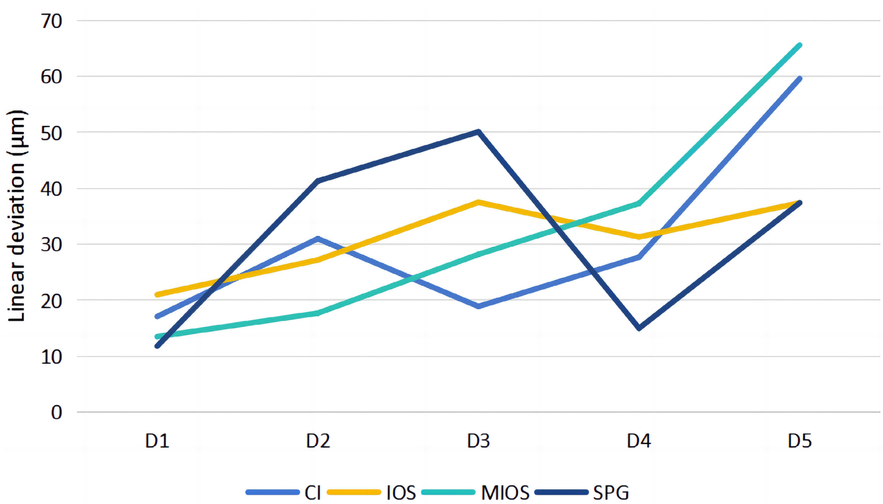

FIGURE 11 Comparing the linear deviation in precision of the individual analog sites across the four impression techniques.

In instances of large defects, this algorithm endeavors to minimize the absolute distance between the two data sets (O'Toole et al., 2019). Although this approach offers the benefit of automatically calculating data differences, it also bears a disadvantage in that the center of each overlap between images varies, which may result in underestimating the true bias (Sanda et al., 2021). To mitigate such errors, our experiment employed the reference best-fit method, which aligns the data set by restricting the alignment to the operator-selected portion of the data set. This technique minimizes alignment errors, facilitating a more accurate measurement (O'Toole et al., 2019).

The IOS technique operates by emitting a light beam, either laser or structured, onto an object. This light is reflected upon reaching the object's surface and is subsequently captured by two or more cameras situated at the scanner's tip. Special processing software generates point clouds, meshes, and 3D coordinates (XYZ axis). These point clouds and meshes are aligned and fused, culminating in a 3D reconstruction of the scanned object (Marques et al., 2021; Zimmermann et al., 2015). Consistent with preceding studies, our research found no significant differences in the overall 3D deviation between the IOS and CI techniques (Marshaha et al., 2023; Papaspyridakos et al., 2016). Analysis of the individual analogs in the model revealed that at the analog of #10, the angular deviation of the CI group was smaller than the IOS group, with other analogs presenting no significant differences. The IOS group exhibited larger linear deviations at D3 compared to the other distances. These results suggest that while CI has minor angular deviations for all analogs, IOS tends to yield larger angular and linear deviations in the cross-arch region. Deviation in the cross-arch region of IOS increases as the scanning range extends due to a dearth of anatomical markers in the edentulous jaw and the progressive error accumulates as images overlap and fuse (Gimenez-Gonzalez et al., 2017; Lyu et al., 2022; Miyoshi et al., 2020; van der Meer et al., 2012). Previous research suggested that the acceptable misfit threshold for implant-supported fixed complete arch prostheses is 50–150 μm and an angular deviation of <0.4° (Andriessen et al., 2014; Di Fiore et al., 2019; Knechtle et al., 2022; Papaspyridakos et al., 2012; Revell et al., 2022; Wulfman et al., 2020). For the present investigation, the 3D deviations of both CI and IOS were more than 50 μm, and their angular deviations exceeded 0.4°. Consequently, neither CI nor IOS provide ideal solutions for capturing impressions for implant-supported fixed complete arch prostheses.

Due to the shortcomings of the IOS technique in creating edentulous dental implant impressions, researchers have proposed the use of artificial markers or auxiliary geometric devices to improve its accuracy. While several studies have confirmed the efficacy of auxiliary geometric devices in enhancing IOS accuracy, Pan et al. (2022) noted that even with these devices, the accuracy of IOS still lagged behind that of CI (Arikan et al., 2023; Iturrate et al., 2019; Masu et al., 2021). These devices also present some challenges: their sizable dimensions interfere with soft tissue recording in edentulous jaws, they necessitate primary impressions for fabrication, and they add to the duration and complexity of the IOS process. Kanjanasavitree et al. (2022) employed three artificial markers to improve IOS accuracy in edentulous jaws, though this manual approach increased the operation time and the markers were susceptible to saliva-induced displacement. Pozzi et al. (2022) developed a non-commercial, 3D-printed splint affixed to a scan body. The resin splint facilitated image stitching and provided a traceable scan path, enhancing the overall accuracy of whole-arch digital impressions. Similarly, Huang et al. (2020) used an extension bar for splinting between scan bodies, achieving IOS impression accuracy comparable to CI. For the present investigation, we utilized commercially available splinting that can be directly attached to the scan body's cross-hole without additional fixation, simplifying the procedure. The results showed comparable overall accuracy between MIOS, IOS, and CI, suggesting that the use of splinting did not enhance the overall accuracy of the IOS technique. While MIOS did decrease the 3D and linear biases at the scan path's commencement compared to IOS and CI, it did not reduce the cumulative error as the scan range expanded.

Stereophotogrammetry is an emerging method for assessing implant positioning in the three-dimensional. It relies on the principle of co-linearity, where object point, image point, and the camera's optical center should coalesce along a straight line. This technique determines implant location by intersecting two different angle images, and its precision depends on image orientation and camera calibration (Rivara et al., 2016). While resistant to environmental light and anatomical landmarks, SPG struggles to capture soft tissue images accurately (Revilla-León et al., 2023). Comparative studies on SPG accuracy in implant-supported fixed complete arch prostheses are limited and yield mixed results. Our study aligns with some findings showing superior SPG accuracy compared to other three techniques (Kosago et al., 2022; Ma et al., 2021; Sallorenzo & Gómez-Polo, 2022; Tohme et al., 2023). However, other research suggests less accuracy, possibly due to 3D printed splints in CIs, which provide enhanced accuracy and distinct measurement methods (Revilla-León et al., 2021, 2023). Some studies reported comparable accuracy between SPG and CI, potentially due to different SPG techniques not directly comparable to our experiment (Bergin et al., 2013; Bratos et al., 2018). In our study, the SPG group displayed minimal angular deviation, remaining within the <0.4° mismatch threshold. This suggests that SPG has potential as a technique for accurately capturing impressions of edentulous jaw implants.

This study recognizes certain limitations particularly the inability of in vitro experiments to entirely simulate the intricacies of the intraoral setting. The aluminum mode used in the present study is different to real patients' arch. This may impact the generalizability of findings to clinical scenarios. Additionally, this investigation did not examine the impact of factors such as implant type, scanning trajectory, or ambient light on the accuracy of the impressions. As a result, future research should delve deeper into how various factors, including implant brands, angular orientations, ambient light conditions, and the presence of saliva, might impact the accuracy of SPG and other IOS techniques.

5 | CONCLUSION

Based on the findings of this in vitro study, the following conclusions were derived:

1. Stereophotogrammetry consistently exhibited superior trueness and precision, with the lowest errors in three-dimensional, angular, and linear measurements.
2. Intraoral scanning did not significantly deviate from the CI. However, it displayed a tendency for angular and linear deviations in the cross-arch region.

3. The inclusion of splinting in the scan body marginally decreased three-dimensional and linear deviations at the start of the scanning path. However, it did not result in an overall accuracy improvement in the accuracy of intraoral scanning.

AUTHOR CONTRIBUTIONS

Jing Cheng: Conceptualization (lead); methodology (lead); writing – original draft (lead); writing – review and editing (lead). **Haidong Zhang**: Conceptualization (lead); methodology (equal); supervision (equal); writing – review and editing (equal). **Hailin Liu**: Data curation (lead); investigation (lead); resources (lead). **Junying Li**: Supervision (equal); writing – original draft (equal); writing – review and editing (equal). **Hom-Lay Wang**: Project administration (equal); supervision (equal); writing – original draft (equal); writing – review and editing (equal). **Xian Tao**: Conceptualization (equal); methodology (equal); supervision (equal); writing – original draft (equal); writing – review and editing (equal).

ACKNOWLEDGMENTS

The authors thank Segma for contributing their material, SKY for their support in terms of implant components, WEGO group for their assistance in the usage of CAD-CAM, and all anonymous reviewers for their insightful comments and constructive suggestions that have elevated this paper to a higher standard.

FUNDING INFORMATION

This work was supported by Natural Science Foundation of Xiamen, China (3502Z202373149; 3502Z202372106), Foundation of stomatological hospital of Xiamen Medical College (2023XKQN0009).

CONFLICT OF INTEREST STATEMENT

The authors declare that they have no known competing financial interests or personal relationships that could have appeared to influence the work reported in this paper.

DATA AVAILABILITY STATEMENT

The data that support the findings of this study are available from the corresponding author upon reasonable request.

ORCID

Hom-Lay Wang https://orcid.org/0000-0003-4238-1799

REFERENCES

al-Turki, L. E. E., Chai, J., Lautenschlager, E. P., & Hutten, M. C. (2002). Changes in prosthetic screw stability because of misfit of implant-supported prostheses. *The International Journal of Prosthodontics*, *15*, 38–42.

Andriessen, F. S., Rijkens, D. R., van der Meer, W. J., & Wismeijer, D. W. (2014). Applicability and accuracy of an intraoral scanner for scanning multiple implants in edentulous mandibles: A pilot study. *The Journal of Prosthetic Dentistry*, *111*, 186–194.

Arcuri, L., Lio, F., Campana, V., Mazzetti, V., Federici, F. R., Nardi, A., & Galli, M. (2022). Influence of implant Scanbody wear on the accuracy of digital impression for complete-arch: A randomized in vitro trial. *Materials (Basel, Switzerland)*, *15*, 927.

Arikan, H., Muhtarogullari, M., Uzel, S. M., Guncu, M. B., Aktas, G., Marshall, L. S., & Turkyilmaz, I. (2023). Accuracy of digital impressions for implant-supported complete-arch prosthesis when using an auxiliary geometry device. *Journal of Dental Sciences*, *18*, 808–813.

Bergin, J. M., Rubenstein, J. E., Mancl, L., Brudvik, J. S., & Raigrodski, A. J. (2013). An in vitro comparison of photogrammetric and conventional complete-arch implant impression techniques. *The Journal of Prosthetic Dentistry*, *110*, 243–251.

Bratos, M., Bergin, J. M., Rubenstein, J. E., & Sorensen, J. A. (2018). Effect of simulated intraoral variables on the accuracy of a photogrammetric imaging technique for complete-arch implant prostheses. *The Journal of Prosthetic Dentistry*, *120*, 232–241.

Daudt Polido, W., Aghaloo, T., Emmett, T. W., Taylor, T. D., & Morton, D. (2018). Number of implants placed for complete-arch fixed prostheses: A systematic review and meta-analysis. *Clinical Oral Implants Research*, *29 Suppl 16*, 154–183.

de Oliveira, N. R. C., Pigozzo, M. N., Sesma, N., & Laganá, D. C. (2020). Clinical efficiency and patient preference of digital and conventional workflow for single implant crowns using immediate and regular digital impression: A meta-analysis. *Clinical Oral Implants Research*, *31*, 669–686.

Di Fiore, A., Meneghello, R., Graiff, L., Savio, G., Vigolo, P., Monaco, C., & Stellini, E. (2019). Full arch digital scanning systems performances for implant-supported fixed dental prostheses: A comparative study of 8 intraoral scanners. *Journal of Prosthodontic Research*, *63*, 396–403.

Dounis, G. S., Ziebert, G. J., & Dounis, K. S. (1991). A comparison of impression materials for complete-arch fixed partial dentures. *The Journal of Prosthetic Dentistry*, *65*, 165–169.

Ellakany, P., Al-Harbi, F., El Tantawi, M., & Mohsen, C. (2022). Evaluation of the accuracy of digital and 3D-printed casts compared with conventional stone casts. *The Journal of Prosthetic Dentistry*, *127*, 438–444.

Filho, H. G., Mazaro, J. V. Q., Vedovatto, E., Assunção, W. G., & dos Santos, P. H. (2009). Accuracy of impression techniques for implants. Part 2 – comparison of splinting techniques. *Journal of Prosthodontics*, *18*, 172–176.

Fluegge, T., Att, W., Metzger, M., & Nelson, K. (2017). A novel method to evaluate precision of optical implant impressions with commercial scan bodies-an experimental approach. *Journal of Prosthodontics*, *26*, 34–41.

Gaikwad, A. M., Joshi, A. A., de Oliveira-Neto, O. B., Padhye, A. M., Nadgere, J. B., Ram, S. M., & Yadav, S. (2022). An overview of systematic reviews and meta-analyses evaluating different impression techniques for implant-supported prostheses in partially and completely edentulous arches. *The International Journal of Oral & Maxillofacial Implants*, *37*, 1119–1137.

Gallardo, Y. R., Bohner, L., Tortamano, P., Pigozzo, M. N., Laganá, D. C., & Sesma, N. (2018). Patient outcomes and procedure working time for digital versus conventional impressions: A systematic review. *The Journal of Prosthetic Dentistry*, *119*, 214–219.

Gimenez-Gonzalez, B., Hassan, B., Özcan, M., & Pradíes, G. (2017). An in vitro study of factors influencing the performance of digital intraoral impressions operating on active wavefront sampling technology with multiple implants in the edentulous maxilla. *Journal of Prosthodontics*, *26*, 650–655.

Hamm, J., Berndt, E. U., Beuer, F., & Zachriat, C. (2020). Evaluation of model materials for CAD/CAM in vitro studies. *International Journal of Computerized Dentistry*, *23*, 49–56.

Huang, R., Liu, Y., Huang, B., Zhang, C., Chen, Z., & Li, Z. (2020). Improved scanning accuracy with newly designed scan bodies: An in vitro study comparing digital versus conventional impression techniques for complete-arch implant rehabilitation. *Clinical Oral Implants Research*, *31*, 625–633.

Imburgia, M., Logozzo, S., Hauschild, U., Veronesi, G., Mangano, C., & Mangano, F. G. (2017). Accuracy of four intraoral scanners in oral implantology: A comparative in vitro study. *BMC Oral Health*, *17*, 92.

ISO 5725-1. (1994). *Accuracy (trueness and precision) of measuring methods and results. Part-I: General principles and definitions*. Beuth Verlag GmbH.

Iturrate, M., Eguiraun, H., Etxaniz, O., & Solaberrieta, E. (2019). Accuracy analysis of complete-arch digital scans in edentulous arches when using an auxiliary geometric device. *The Journal of Prosthetic Dentistry*, *121*, 447–454.

Jemt, T. (2017). A retro-prospective effectiveness study on 3448 implant operations at one referral clinic: A multifactorial analysis. Part I: Clinical factors associated to early implant failures. *Clinical Implant Dentistry and Related Research*, *19*, 980–988.

Jemt, T. (2018). Implant survival in the edentulous Jaw-30 years of experience. Part I: A retro-prospective multivariate regression analysis of overall implant failure in 4,585 consecutively treated arches. *The International Journal of Prosthodontics*, *31*, 425–435.

Jemt, T., Bäck, T., & Petersson, A. (1999). Photogrammetry--an alternative to conventional impressions in implant dentistry? A clinical pilot study. *The International Journal of Prosthodontics*, *12*, 363–368.

Jin, S., Kim, D., Kim, J., & Kim, W. (2019). Accuracy of dental replica models using photopolymer materials in additive manufacturing: In vitro three-dimensional evaluation. *Journal of Prosthodontics*, *28*, e557–e562.

Kanjanasavitree, P., Thammajaruk, P., & Guazzato, M. (2022). Comparison of different artificial landmarks and scanning patterns on the complete-arch implant intraoral digital scans. *Journal of Dentistry*, *125*, 104266.

Katsoulis, J., Takeichi, T., Sol Gaviria, A., Peter, L., & Katsoulis, K. (2017). Misfit of implant prostheses and its impact on clinical outcomes. Definition, assessment and a systematic review of the literature. *European Journal of Oral Implantology*, *10 Suppl 1*, 121–138.

Knechtle, N., Wiedemeier, D., Mehl, A., & Ender, A. (2022). Accuracy of digital complete-arch, multi-implant scans made in the edentulous jaw with gingival movement simulation: An in vitro study. *The Journal of Prosthetic Dentistry*, *128*, 468–478.

Kosago, P., Ungurawasaporn, C., & Kukiattrakoon, B. (2022). Comparison of the accuracy between conventional and various digital implant impressions for an implant-supported mandibular complete arch-fixed prosthesis: An in vitro study. *Journal of Prosthodontics*, *32*, 616–624. https://doi.org/10.1111/jopr.13604

Lambert, F. E., Weber, H. P., Susarla, S. M., Belser, U. C., & Gallucci, G. O. (2009). Descriptive analysis of implant and prosthodontic survival rates with fixed implant-supported rehabilitations in the edentulous maxilla. *Journal of Periodontology*, *80*, 1220–1230.

Lyu, M., Di, P., Lin, Y., & Jiang, X. (2022). Accuracy of impressions for multiple implants: A comparative study of digital and conventional techniques. *The Journal of Prosthetic Dentistry*, *128*, 1017–1023.

Ma, B., Yue, X., Sun, Y., Peng, L., & Geng, W. (2021). Accuracy of photogrammetry, intraoral scanning, and conventional impression techniques for complete-arch implant rehabilitation: An in vitro comparative study. *BMC Oral Health*, *21*, 636.

Marques, S., Ribeiro, P., Falcão, C., Lemos, B. F., Ríos-Carrasco, B., Ríos-Santos, J. V., & Herrero-Climent, M. (2021). Digital impressions in implant dentistry: A literature review. *International Journal of Environmental Research and Public Health*, *18*, 1020.

Marshaha, N. J., Azhari, A. A., Assery, M. K., & Ahmed, W. M. (2023). Evaluation of the trueness and precision of conventional impressions versus digital scans for the all-on-four treatment in the maxillary arch: An in vitro study. *Journal of Prosthodontics*, *22*, 171–179.

Masu, R., Tanaka, S., Sanda, M., Miyoshi, K., & Baba, K. (2021). Effect of assistive devices on the precision of digital impressions for implants placed in edentulous maxilla: An in vitro study. *International Journal of Implant Dentistry*, *7*, 116.

Miyoshi, K., Tanaka, S., Yokoyama, S., Sanda, M., & Baba, K. (2020). Effects of different types of intraoral scanners and scanning ranges on the precision of digital implant impressions in edentulous maxilla: An in vitro study. *Clinical Oral Implants Research*, *31*, 74–83.

Mizumoto, R. M., Yilmaz, B., McGlumphy, E. A. J., Seidt, J., & Johnston, W. M. (2020). Accuracy of different digital scanning techniques and scan bodies for complete-arch implant-supported prostheses. *The Journal of Prosthetic Dentistry*, *123*, 96–104.

Müller, P., Ender, A., Joda, T., & Katsoulis, J. (2016). Impact of digital intraoral scan strategies on the impression accuracy using the TRIOS Pod scanner. *Quintessence International*, *47*, 343–349.

Ochoa-López, G., Cascos, R., Antonaya-Martín, J. L., Revilla-León, M., & Gómez-Polo, M. (2022). Influence of ambient light conditions on the accuracy and scanning time of seven intraoral scanners in complete-arch implant scans. *Journal of Dentistry*, *121*, 104138.

Ortorp, A., Jemt, T., & Bäck, T. (2005). Photogrammetry and conventional impressions for recording implant positions: A comparative laboratory study. *Clinical Implant Dentistry and Related Research*, *7*, 43–50.

O'Toole, S., Osnes, C., Bartlett, D., & Keeling, A. (2019). Investigation into the accuracy and measurement methods of sequential 3D dental scan alignment. *Dental Materials*, *35*, 495–500.

Pan, Y., Tam, J. M. Y., Tsoi, J. K. H., Lam, W. Y. H., & Pow, E. H. N. (2020). Reproducibility of laboratory scanning of multiple implants in complete edentulous arch: Effect of scan bodies. *Journal of Dentistry*, *96*, 103329.

Pan, Y., Tsoi, J. K. H., Lam, W. Y. H., & Pow, E. H. N. (2021). Implant framework misfit: A systematic review on assessment methods and clinical complications. *Clinical Implant Dentistry and Related Research*, *23*, 244–258.

Pan, Y., Tsoi, J. K. H., Lam, W. Y. H., Zhao, K., & Pow, E. H. N. (2022). The cumulative effect of error in the digital workflow for complete-arch implant-supported frameworks: An in vitro study. *Clinical Oral Implants Research*, *33*, 886–899.

Papaspyridakos, P., Benic, G. I., Hogsett, V. L., White, G. S., Lal, K., & Gallucci, G. O. (2012). Accuracy of implant casts generated with splinted and non-splinted impression techniques for edentulous patients: An optical scanning study. *Clinical Oral Implants Research*, *23*, 676–681.

Papaspyridakos, P., Gallucci, G. O., Chen, C. J., Hanssen, S., Naert, I., & Vandenberghe, B. (2016). Digital versus conventional implant impressions for edentulous patients: Accuracy outcomes. *Clinical Oral Implants Research*, *27*, 465–472.

Papaspyridakos, P., Mokti, M., Chen, C. J., Benic, G. I., Gallucci, G. O., & Chronopoulos, V. (2014). Implant and prosthodontic survival rates with implant fixed complete dental prostheses in the edentulous mandible after at least 5 years: A systematic review. *Clinical Implant Dentistry and Related Research*, *16*, 705–717.

Patzelt, S. B. M., Emmanouilidi, A., Stampf, S., Strub, J. R., & Att, W. (2014). Accuracy of full-arch scans using intraoral scanners. *Clinical Oral Investigations*, *18*, 1687–1694.

Peñarrocha-Oltra, D., Agustín-Panadero, R., Pradíes, G., Gomar-Vercher, S., & Peñarrocha-Diago, M. (2017). Maxillary full-arch immediately loaded implant-supported fixed prosthesis designed and produced by photogrammetry and digital printing: A clinical report. *Journal of Prosthodontics*, *26*, 75–81.

Pozzi, A., Arcuri, L., Lio, F., Papa, A., Nardi, A., & Londono, J. (2022). Accuracy of complete-arch digital implant impression with or without scanbody splinting: An in vitro study. *Journal of Dentistry*, *119*, 104072.

Revell, G., Simon, B., Mennito, A., Evans, Z. P., Renne, W., Ludlow, M., & Vág, J. (2022). Evaluation of complete-arch implant scanning with 5 different intraoral scanners in terms of trueness and operator experience. *The Journal of Prosthetic Dentistry*, *128*, 632–638.

Revilla-León, M., Att, W., Özcan, M., & Rubenstein, J. (2021). Comparison of conventional, photogrammetry, and intraoral scanning accuracy of complete-arch implant impression procedures evaluated with a coordinate measuring machine. *The Journal of Prosthetic Dentistry*, *125*, 470–478.

Revilla-León, M., Rubenstein, J., Methani, M. M., Piedra-Cascón, W., Özcan, M., & Att, W. (2023). Trueness and precision of complete-arch photogrammetry implant scanning assessed with a coordinate-measuring machine. *The Journal of Prosthetic Dentistry*, *129*, 160–165.

Rivara, F., Lumetti, S., Calciolari, E., Toffoli, A., Forlani, G., & Manfredi, E. (2016). Photogrammetric method to measure the discrepancy between clinical and software-designed positions of implants. *The Journal of Prosthetic Dentistry*, *115*, 703–711.

Sallorenzo, A., & Gómez-Polo, M. (2022). Comparative study of the accuracy of an implant intraoral scanner and that of a conventional intraoral scanner for complete-arch fixed dental prostheses. *The Journal of Prosthetic Dentistry*, *128*, 1009–1016.

Sánchez-Monescillo, A., Sánchez-Turrión, A., Vellon-Domarco, E., Salinas-Goodier, C., & Prados-Frutos, J. C. (2016). Photogrammetry impression technique: A case history report. *The International Journal of Prosthodontics*, *29*, 71–73.

Sanda, M., Miyoshi, K., & Baba, K. (2021). Trueness and precision of digital implant impressions by intraoral scanners: A literature review. *International Journal of Implant Dentistry*, *7*, 97.

Schimmel, M., Akino, N., Srinivasan, M., Wittneben, J. G., Yilmaz, B., & Abou-Ayash, S. (2021). Accuracy of intraoral scanning in completely and partially edentulous maxillary and mandibular jaws: An in vitro analysis. *Clinical Oral Investigations*, *25*, 1839–1847.

Slauch, R. W., Bidra, A. S., Wolfinger, G. J., & Kuo, C. L. (2019). Relationship between radiographic misfit and clinical outcomes in immediately loaded complete-arch fixed implant-supported prostheses in edentulous patients. *Journal of Prosthodontics*, *28*, 861–867.

Tohme, H., Lawand, G., Chmielewska, M., & Makhzoume, J. (2023). Comparison between stereophotogrammetric, digital, and conventional impression techniques in implant-supported fixed complete arch prostheses: An in vitro study. *The Journal of Prosthetic Dentistry*, *129*, 354–362.

Toia, M., Stocchero, M., Jinno, Y., Wennerberg, A., Becktor, J. P., Jimbo, R., & Halldin, A. (2019). Effect of misfit at implant-level framework and supporting bone on internal connection implants: Mechanical and finite element analysis. *The International Journal of Oral & Maxillofacial Implants*, *34*, 320–328.

van der Meer, W. J., Andriessen, F. S., Wismeijer, D., & Ren, Y. (2012). Application of intra-oral dental scanners in the digital workflow of implantology. *PLoS One*, *7*, e43312.

Wulfman, C., Naveau, A., & Rignon-Bret, C. (2020). Digital scanning for complete-arch implant-supported restorations: A systematic review. *The Journal of Prosthetic Dentistry*, *124*, 161–167.

Yuzbasioglu, E., Kurt, H., Turunc, R., & Bilir, H. (2014). Comparison of digital and conventional impression techniques: Evaluation of patients' perception, treatment comfort, effectiveness and clinical outcomes. *BMC Oral Health*, *14*, 10.

Zhang, S., Chen, W., Lin, Y., & Chen, J. (2023). A digital technique for transferring the maxillomandibular relationship for complete arch implant rehabilitation in edentulous jaws. *The Journal of Prosthetic Dentistry*, S0022-3913(22)00494-2.

Zhang, Y. J., Shi, J. Y., Qian, S. J., Qiao, S. C., & Lai, H. C. (2021). Accuracy of full-arch digital implant impressions taken using intraoral scanners and related variables: A systematic review. *International Journal of Oral Implantology (Berlin, Germany)*, *14*, 157–179.

Zhou, L., Luo, Y., Zhang, Z., He, M., Xu, Y., Zhao, Y., Liu, S., Dong, L., & Zhang, Z. (2021). Microstructures and macrosegregation of Al–Zn–Mg–Cu alloy billet prepared by uniform direct chill casting. *Materials (Basel, Switzerland)*, *14*, 708.

Zimmermann, M., Mehl, A., Mörmann, W. H., & Reich, S. (2015). Intraoral scanning systems - a current overview. *International Journal of Computerized Dentistry*, *18*, 101–129.

SUPPORTING INFORMATION

Additional supporting information can be found online in the Supporting Information section at the end of this article.

How to cite this article: Cheng, J., Zhang, H., Liu, H., Li, J., Wang, H.-L., & Tao, X. (2024). Accuracy of edentulous full-arch implant impression: An in vitro comparison between conventional impression, intraoral scan with and without splinting, and photogrammetry. *Clinical Oral Implants Research*, *35*, 560–572. https://doi.org/10.1111/clr.14252